MATHEMATICAL SCIENCES AND APPLICATIONS E-NOTES
https://doi.org/10.36753/mathenot.1695610
13 (3) 126-143 (2025) - Research Article
ISSN: 2147-6268

A Comprehensive Evaluation of the Impact of Mask-Wearing on COVID-19 Transmission Dynamics: A Fractional Calculus Approach to Understanding Public Health Dynamics

Elif Demir* and Canan Vural

Abstract
The COVID-19 pandemic exposed vulnerabilities in global public health systems, emphasizing the urgent need for effective interventions. Among these, mask-wearing has proven to be a critical measure in reducing viral transmission by limiting respiratory droplet spread. To quantitatively evaluate the impact of mask usage, this study develops a fractional SIR model incorporating mask protection efficiency and mask-wearing rates for both susceptible and infected populations. The model utilizes the Caputo fractional derivative to better capture memory effects in disease transmission dynamics. Stability analysis is conducted, and the basic reproduction number is derived to assess the model's behavior under varying conditions. The fractional forward Euler method is applied to approximate the system's solutions, and numerical simulations are performed using MATLAB. Real COVID-19 data from Türkiye, spanning April 21–30, 2021, is employed to estimate mask-wearing rates, combined with actual demographic statistics and average mask efficacy values. The results highlight the significant role of mask efficiency and adherence in reducing disease spread, with visualizations providing insights into the effects of parameter variations. This study underscores the critical importance of mask-wearing as a non-pharmaceutical intervention and demonstrates the applicability of fractional calculus in epidemiological modeling.

Keywords: *Caputo type fractional derivative, Fractional SIR model, Mask protection efficiency, Transmission of COVID-19*

AMS Subject Classification (2020): *37N25; 26A33; 34A12*

*Corresponding author

Received : *08-05-2025,* ***Accepted :*** *25-07-2025,* ***Available online :*** *30-07-2025*

(***Cite as*** *"E. Demir, C. Vural, A Comprehensive Evaluation of the Impact of Mask-Wearing on COVID-19 Transmission Dynamics: A Fractional Calculus Approach to Understanding Public Health Dynamics, Math. Sci. Appl. E-Notes, 13(3) (2025), 126-143")*

1. Introduction

In recent years, the world has faced a significant challenge: COVID-19. This infectious disease is transmitted from person to person and was first identified in late December 2019 in Wuhan, China. The virus was officially recognized on January 13, 2020. On January 30, 2020, the World Health Organization (WHO) declared COVID-19 a global health emergency, and on March 11, 2020, it was designated as a pandemic. A pandemic refers to the widespread transmission of a disease or infection across countries, continents, and ultimately, the entire globe. In Türkiye, initial studies on COVID-19 commenced on January 10, 2020, when the Republic of Türkiye Ministry of Health's Scientific Advisory Board held its first meeting regarding the virus. The first confirmed case of COVID-19 in Türkiye was reported on March 11, 2020 [1].

COVID-19 is primarily transmitted through respiratory droplets. When an infected individual coughs, droplets are released into the environment, and subsequent inhalation of these droplets can lead to infection in others. Additionally, individuals may become infected if they touch their face, eyes, nose, or mouth with unwashed hands after coming into contact with surfaces contaminated by respiratory droplets from infected persons [2].

As COVID-19 cases rose, new terminology and habits emerged, including the concepts of masks, social distancing, and hygiene. Several precautions are essential for mitigating the spread of the virus. Given that COVID-19 is transmitted via respiratory droplets, the use of masks is critical. Furthermore, since the virus can also survive on surfaces, regular hand washing is another vital measure. Hands should be washed with soap whenever possible; in the absence of soap, hand sanitizers containing antiseptic can be utilized. Another important precaution is to minimize contact with infected individuals, maintaining a minimum distance of at least 1.5 meters from them [3]. To adhere to this guideline, it is advisable to avoid crowded places.

An important consideration when wearing a mask is ensuring it is worn correctly. Prior to donning a mask, it is essential to disinfect hands and wash them thoroughly with soap for at least 20 seconds. The mask should fully cover both the mouth and nose, with no gaps between the mask and the face. It is advisable to avoid touching the exterior surface of the mask; if contact occurs, hands should be disinfected immediately. Additionally, if the mask becomes damp, it should be replaced with a new one. Reusing disposable masks is strongly discouraged [4].

Not all masks provide the same level of protection; their efficacy varies based on factors such as the size of viral particles, the materials used in the mask, and other design considerations. Therefore, making an informed choice regarding mask selection is crucial. The most commonly used masks for protection against COVID-19 include N95 respirators, surgical masks, and cloth masks. Among these, N95 respirators offer the highest filtration efficiency, achieving approximately 95% effectiveness for particles larger than 300 nm [5]. Research indicates that the infection rates associated with N95 masks and surgical masks are comparable. In contrast, cloth masks demonstrate significantly lower filtration efficiency compared to the other types, rendering them the least effective option for preventing transmission.

This paper investigates the relationship between the numbers of susceptible (S), infected (I), and recovered (R) individuals in relation to varying rates of mask-wearing and mask efficacy, employing a fractional SIR model. The concept of fractional derivatives originated from Leibniz's response to L'Hôpital's inquiry regarding the implications of setting $n = \frac{1}{2}$ in the expression $\frac{D^n f(x)}{Dx^n}$, which was posed in a letter dated September 30, 1695 [6]. Numerous researchers have utilized fractional derivatives within their SIR models, as we have in this study [7–10]. These models find extensive applications across various disciplines, including biology [11, 12], chemistry [13, 14], physics [15, 16], and engineering [17, 18]. In [19], a mathematical model with Caputo fractional derivative was used to study social media addiction, without adopting the classical SIR formulation. This highlights the versatility of fractional calculus in modeling diverse dynamic systems.

The increasing popularity of fractional models can be attributed to their ability to provide more accurate approximations of real-world data compared to classical models. In this article, fractional derivatives are employed for data fitting using actual COVID-19 data from Türkiye. Researchers in this field have conducted data fitting and analyses for various scenarios using COVID-19 data from multiple countries. For instance, in [20], COVID-19 data from Türkiye was analyzed using a hybrid SARIMA-NNAR model combining statistical and neural network approaches. Furthermore, the study in [21] focused on the global dynamics of COVID-19 and employed the SIRD model for the analysis. Some studies have utilized the original fractional models, as we have, while others have implemented the classical SIR model. For instance, the article [22] performs data fitting with real data from Türkiye and presents comparisons based on different parameter values, employing the Atangana-Baleanu (AB) fractional derivative. Similarly, the authors in [23] utilized real COVID-19 data from Italy and compared it with predictions generated by the classical SIR model. In the study presented in [24], parameter estimation was conducted using COVID-19 data from India during lockdown periods. These articles exemplify the application of classical models to analyze real COVID-19 data across various countries.

In the article [25], COVID-19 dynamics across various countries are analyzed using a fractional SIR model, with the findings illustrated through graphical representations. The authors of article [26] employed a fractional SIR model that incorporates a vaccination rate parameter, underscoring the critical role of vaccination in mitigating epidemic diseases. Additionally, article [27] presents a model that features nonlinear incidence and recovery rates, accompanied by various studies illustrated through graphics. These cited articles represent significant contributions to the field, exploring epidemic diseases through the application of fractional SIR models worldwide. In our study, we have modified the classical SIR model by integrating parameters such as mask-wearing rates and mask protection efficiency. This modification elucidates the effects of mask usage and the efficacy of different masks on the trajectory of the pandemic, supported by numerical results and graphical analyses. Furthermore, our examination and data fitting utilize real COVID-19 data from Türkiye.

2. Overview of the model and its parameters

[36] This article introduces a model that characterizes the dynamics of Covid-19, incorporating parameters related to mask usage. The model utilizes a Caputo-type fractional derivative to effectively capture the essential dynamics of the situation.

In this model, the total population N is assumed to be constant. The population is classified into three compartments: susceptible (denoted as S), infected (denoted as I), and recovered (denoted as R). The functions $S(t)$, $I(t)$, and $R(t)$ represent the number of individuals in each compartment at a given time t. Consequently, the equation $S(t) + I(t) + R(t) = N$ is maintained throughout the analysis.

Fundamental Assumptions of the Model :

- **Assumption 1 :** It is assumed that the birth and death rates are equal.
- **Assumption 2 :** It is required that the number of individuals in the susceptible (S), infected (I), and recovered (R) compartments remains non-negative at all times.
- **Assumption 3 :** All parameters within the model are required to be bounded between 0 and 1.

Parameters In The Model	**Definitions**
μ	Birth rate and death rate
β	Contact rate between susceptible people and infected people
e	Rate of mask protection efficiency
u	Rate of wearing mask of susceptible people
v	Rate of wearing mask of infected people
γ	Recovery rate
α	Order of the fractional derivatives

Table 1. Parametric Framework of the Model

Table 1 provides a detailed listing of the parameters utilized in the model, along with their respective definitions.

This model pertains to the use of masks, encompassing four distinct scenarios based on the mask-wearing behaviors of susceptible and infected individuals.

Situation 1: Assume that susceptible individuals without masks are in contact with infected individuals wearing masks. In this scenario, a number

$$\frac{(1-e)(1-u)v\beta}{N}SI$$

of susceptible individuals transitions into the infected group.

Situation 2: Assume that susceptible individuals without masks are in contact with infected individuals without masks. In this scenario, a number

$$\frac{(1-u)(1-v)\beta}{N}SI$$

of susceptible individuals transitions into the infected group.

Situation 3: Assume that susceptible individuals wearing masks are in contact with infected individuals wearing masks. In this scenario, a number

$$\frac{(1-e)uv\beta}{N}SI$$

of susceptible individuals transitions into the infected group.

Situation 4: Assume that susceptible individuals wearing masks are in contact with infected individuals without masks. In this scenario, a number

$$\frac{(1-e)u(1-v)\beta}{N}SI$$

of susceptible individuals transitions into the infected group.

Utilizing these assumptions and scenarios, the following model is derived, which incorporates rates of mask protection efficiency and mask-wearing behavior:

$$\begin{aligned} {}^{C}D_t^{\alpha}S &= \mu N - \mu S - \frac{[1-e(u+v-uv)]\beta}{N}SI \\ {}^{C}D_t^{\alpha}I &= \frac{[1-e(u+v-uv)]\beta}{N}SI - (\mu+\gamma)I \\ {}^{C}D_t^{\alpha}R &= \gamma I - \mu R \end{aligned} \tag{2.1}$$

with S(0) = S_0 >0 , I(0) = I_0 >0 and R(0) = R_0 >0 initial conditions .

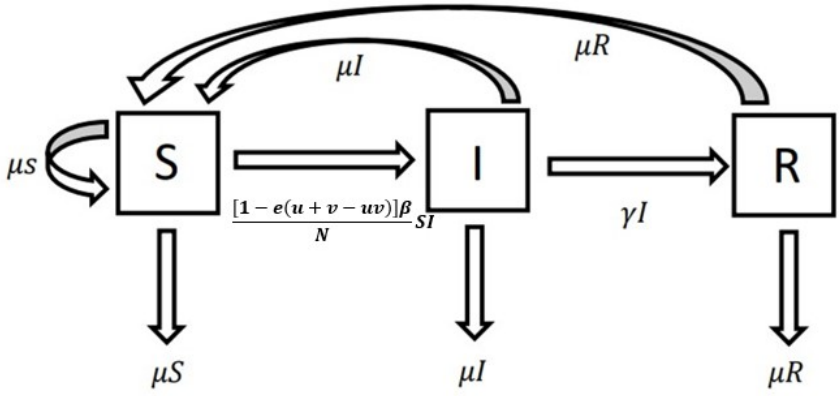

Figure 1. Diagram Illustrating the Model Dynamics

3. Analysis of solution

3.1 Non-negativity of solution

Let $\mathbb{R}^3_+$={$F \in \mathbb{R}^3 : F \geq 0$} and $F(t) = (F_1(t), F_2(t), F_3(t))^T$. Lemma and Corollary are used to prove the theorems about non-negativity of solutions [26] and also the same approaches used in [37] are implemented.

Lemma 3.1. ***(Generalized Mean Value Theorem):*** *Assume that $f(t)$ and $D^{\alpha}f(t)$ are continuous functions in the closed interval $[a_1, a_2]$ for $0 < \alpha \leq 1$. Then for all t in $[a_1, a_2]$, $f(t) = f(a_1) + \frac{1}{\Gamma\alpha}D^{\alpha}f(\xi)(t-a_1)^{\alpha}$ holds with $0 \geq \xi \geq t$. [28] .*

Corollary 3.1. *Assume that f(t) and $D^{\alpha}f(t)$ are continuous functions in the closed interval [0,a] for $0 < \alpha \leq 1$. It can be seen easily from Lemma that if $D^{\alpha}f(t) \geq 0$ holds for all t in the open interval (0,a), then f(t) is nondecreasing for all t in the closed interval [0,a]. Also if $D^{\alpha}f(t) \leq 0$ holds forall t in the open interval (0,a), then f(t) is nonincreasing for all t in the closed interval [0,a]. [26].*

Theorem 3.1. *Let $F(t) = (S(t), I(t), R(t))^T$ be the solution of the problem (1) and S(0) = S_0 >0 , I(0) = I_0 >0 , R(0) = R_0 >0. Then $F(t) \in \mathbb{R}^3_+$={$F \in \mathbb{R}^3 : F \geq 0$}.*

Proof. Showing that $\mathbb{R}^3_+$ is positively invariant is necessary to prove.
${}^C D_t^\alpha S(t)|_{S=0} = \mu N \geq 0$,
${}^C D_t^\alpha I(t)|_{I=0} = 0$,
${}^C D_t^\alpha R(t)|_{R=0} = \gamma I - \mu R \geq 0$,
So by the corollary, on each hyperplane bounding the non-negative octant, the vector field point into $\mathbb{R}^3_+$. □

3.2 Existence and uniqueness of solution

In order to simplify the expression of model (2.1), we define the following notations:
$k(t) = \frac{[1-e(u+v-uv)]\beta}{N} I$, $m = \mu + \gamma$.

$$\begin{aligned} {}^C D_t^\alpha S &= \mu N - \mu S - k(t)S \\ {}^C D_t^\alpha I &= k(t)S - mI \\ {}^C D_t^\alpha R &= \gamma I - \mu R. \end{aligned} \tag{3.1}$$

As a first step in analyzing the system (3.1) with its initial conditions, we demonstrate the existence and uniqueness of solutions by applying fixed point theory together with the Picard–Lindelöf technique. This analysis calls for the use of the Caputo fractional integral operator introduced in [38].

$${}_0^C I_t^\alpha T(t) = \frac{1}{\Gamma(\alpha)} \int_0^t \frac{T(p)}{(t-p)^{1-\alpha}} dp.$$

After being applied to both sides of the system (3.1), the operator is used—together with the definition of the Caputo derivative [31],

$${}^C D_t^\alpha f(t) = \tfrac{1}{\Gamma(1-\alpha)} \textstyle\int_0^t (t-s)^{-\alpha} f'(s) ds, \quad \alpha \in (0,1).$$

to rewrite the system in an integral form. This reformulation is instrumental for the next steps of the analysis:

$$\begin{aligned} S(t) - S(0) &= {}_0^C I_t^\alpha \{\mu N - \mu S - k(t)S\} \\ I(t) - I(0) &= {}_0^C I_t^\alpha \{k(t)S - mI\} \\ R(t) - R(0) &= {}_0^C I_t^\alpha \{\gamma I - \mu R\} \end{aligned} \tag{3.2}$$

To facilitate a simplified form, the system presented in (3.2) is expressed in terms of kernels.

$$\begin{aligned} S(t) - S(0) &= \frac{1}{\Gamma(\alpha)} \int_0^t K_1(p,S)(t-p)^{\alpha-1} dp \\ I(t) - I(0) &= \frac{1}{\Gamma(\alpha)} \int_0^t K_2(p,I)(t-p)^{\alpha-1} dp \\ R(t) - R(0) &= \frac{1}{\Gamma(\alpha)} \int_0^t K_3(p,R)(t-p)^{\alpha-1} dp. \end{aligned} \tag{3.3}$$

The kernels mentioned above are explicitly expressed as:

$$\begin{aligned} K_1(t,S) &= \mu N - \mu S - k(t)S, \\ K_2(t,I) &= k(t)S - mI, \\ K_3(t,R) &= \gamma I - \mu R. \end{aligned}$$

Moreover, applying Picard iterations yields the following recursive relations:

$$S^{n+1}(t) = \frac{1}{\Gamma(\alpha)} \int_0^t K_1(p,S^n)(t-p)^{\alpha-1} dp$$

$$I^{n+1}(t) = \frac{1}{\Gamma(\alpha)} \int_0^t K_2(p,I^n)(t-p)^{\alpha-1} dp$$

$$R^{n+1}(t) = \frac{1}{\Gamma(\alpha)} \int_0^t K_3(p, R^n)(t-p)^{\alpha-1} dp.$$

In the following step, the system in (3.1) is reformulated as:

$$ {}_0^C D_t^\alpha \mathscr{Y}(t) = H(t, \mathscr{Y}(t)), \quad \mathscr{Y}(0) = \mathscr{Y}_0, \quad 0 < t < T \tag{3.4}$$

where $\mathscr{Y}(t)$ denotes the vector function defined by:

$$\mathscr{Y}(t) = (S(t), I(t), R(t))^T$$

and the expression for the vector function $H(t, \mathscr{Y}(t))$ is given by:

$$H(t, \mathscr{Y}(t)) = \begin{pmatrix} \mu N - \mu S - k(t)S \\ k(t)S - mI \\ \gamma I - \mu R \end{pmatrix}.$$

and $\mathscr{Y}_0 = (S(0), I(0), R(0))^T$.

By considering (3.3) in connection with (3.4), the corresponding integral equation is expressed as:

$$\mathscr{Y}(t) = \mathscr{Y}_0 + \frac{1}{\Gamma(\alpha)} \int_0^t H(s, \mathscr{Y}(s)) ds. \tag{3.5}$$

Theorem 3.2. *Let $\Omega = [0, T]$, and suppose that $\mathscr{Y}(t) \in C(\Omega, \mathbb{R}^3)$. Then, the following Lipschitz condition is satisfied: There exists a constant $L > 0$ such that*

$$||H(t, \mathscr{Y}_1(t)) - H(t, \mathscr{Y}_2(t))|| \leq L||\mathscr{Y}_1(t) - \mathscr{Y}_2(t)||$$

for all $\mathscr{Y}_1(t), \mathscr{Y}_2(t) \in C(\Omega, \mathbb{R}^3)$ and for every $t \in \Omega$.

Proof.

$$||H(t, \mathscr{Y}_1(t)) - H(t, \mathscr{Y}_2(t))|| = \begin{pmatrix} ||K_1(t, S_1) - K_1(t, S_2)|| \\ ||K_2(t, I_1) - K_2(t, I_2)|| \\ ||K_3(t, R_1) - K_3(t, R_2)|| \end{pmatrix}$$

$$\begin{pmatrix} ||\mu + k(t)||\, ||S_1(t) - S_2(t)|| \\ m||I_1(t) - I_2(t)|| \\ \mu||R_1(t) - R_2(t)|| \end{pmatrix} = \begin{pmatrix} \mathscr{A}_1 & 0 & 0 \\ 0 & \mathscr{A}_2 & 0 \\ 0 & 0 & \mathscr{A}_3 \end{pmatrix} \times ||\mathscr{Y}_1(t) - \mathscr{Y}_2(t)||$$

$$= \mathscr{A}||\mathscr{Y}_1(t) - \mathscr{Y}_2(t)||,$$

where $\mathscr{A}_1 = ||\mu + k(t)||$, $\mathscr{A}_2 = m$, $\mathscr{A}_3 = \mu$. Consequently,

$$\begin{aligned} ||H(t, \mathscr{Y}_1(t)) - H(t, \mathscr{Y}_2(t))|| &\leq \sup_{||x|| < 1} ||\mathscr{A}x|| \\ &\leq L||\mathscr{Y}_1(t) - \mathscr{Y}_2(t)||, \end{aligned}$$

where

$$L = max(sup\mathscr{A}_1, sup\mathscr{A}_2, sup\mathscr{A}_3).$$

□

Theorem 3.3. *The system of equations given in (3.1) admits a unique solution provided that the following condition holds:*

$$\frac{1}{\Gamma(\alpha)} L \frac{T^\alpha}{\alpha} < 1.$$

Proof. Let the mapping $\Pi : \mathcal{C}(\Omega, \mathbb{R}^3) \to \mathcal{C}(\Omega, \mathbb{R}^3)$ be defined by

$$\Pi(\mathscr{Y}(t)) = \mathscr{Y}_0 + \frac{1}{\Gamma(\alpha)} \int_0^t H(s, \mathscr{Y}(s))(t-s)^{\alpha-1} ds.$$

Accordingly, equation (3.5) is reformulated in terms of the operator Π as

$$\mathscr{Y}(t) = \Pi(\mathscr{Y}(t)).$$

The space $\mathcal{C}(\Omega, \mathbb{R}^3)$, defined as the set of all continuous vector-valued functions on Ω, becomes a Banach space under the norm $||a||_{\mathcal{C}} = \sup_{t\in\Omega} |a(t)|$.
From equation (3.5), the following relations can be derived:

$$\begin{aligned}
||\Pi(\mathscr{Y}_1(t)) - \Pi(\mathscr{Y}_2(t))||_{\mathcal{C}} &= ||\frac{1}{\Gamma(\alpha)}\int_0^t (H(s,\mathscr{Y}_1(s) - H(\mathscr{Y}_2(s)))(t-s)^{\alpha-1}ds||_{\mathcal{C}} \\
&\leq \frac{1}{\Gamma(\alpha)}\int_0^t ||(H(s,\mathscr{Y}_1(s) - H(\mathscr{Y}_2(s)))(t-s)^{\alpha-1}||_{\mathcal{C}}\, ds \\
&\leq \frac{1}{\Gamma(\alpha)} L \int_0^t ||\mathscr{Y}_1(s) - \mathscr{Y}_2(s)||_{\mathcal{C}} ||(t-s)^{\alpha-1}||_{\mathcal{C}}\, ds \\
&\leq \frac{1}{\Gamma(\alpha)} L \max_{t\in\Omega}\Big(\frac{t^\alpha}{\alpha}\Big) ||\mathscr{Y}_1(t) - \mathscr{Y}_2(t)||_{\mathcal{C}} \\
&= \frac{1}{\Gamma(\alpha)} L \frac{T^\alpha}{\alpha} ||\mathscr{Y}_1(t) - \mathscr{Y}_2(t)||_{\mathcal{C}}.
\end{aligned}$$

Under the condition $\frac{1}{\Gamma(\alpha)} L \frac{T^\alpha}{\alpha} < 1$, the mapping Π becomes a contraction on the Banach space $\mathcal{C}(\Omega, \mathbb{R}^3)$. Consequently, the system of equations given in (3.1) possesses a unique solution. □

4. Stability analysis of the model

Equilibrium points of the model are $(\overline{S}, \overline{I}, \overline{R})$ which are solutions of the following system of equations :

$$\mu N - \mu\overline{S} - \frac{[1-e(u+v-uv)]\beta}{N}\overline{SI} = 0$$

$$\frac{[1-e(u+v-uv)]\beta}{N}\overline{SI} - (\mu+\gamma)\overline{I} = 0$$

$$\gamma\overline{I} - \mu\overline{R} = 0$$

The equilibrium points that found for this model, the first being the disease free equilibrium point and the second being the endemic equilibrium point, are as follows :

- $E_1 = (N, 0, 0)$
- $E_2 = \Big(\frac{N(\mu+\gamma)}{[1-e(u+v-uv)]\beta}, N\big(\frac{\mu}{\mu+\gamma} - \frac{\mu}{[1-e(u+v-uv)]\beta}\big), N\big(\frac{\gamma}{\mu+\gamma} - \frac{\gamma}{[1-e(u+v-uv)]\beta}\big)\Big)$

The Jacobian matrix for the model is obtained in the following form :

$$\mathbf{J} = \begin{pmatrix} -\mu - \frac{[1-e(u+v-uv)]\beta}{N} I & -\frac{[1-e(u+v-uv)]\beta}{N} S & 0 \\ \frac{[1-e(u+v-uv)]\beta}{N} I & \frac{[1-e(u+v-uv)]\beta}{N} S - (\mu+\gamma) & 0 \\ 0 & \gamma & -\mu \end{pmatrix}.$$

Stability Conditions For E_1 : The Jacobian matrix is evaluated at E_1 in the following form :

$$\mathbf{J}|_{\mathbf{E_1}} = \begin{pmatrix} -\mu & -[1-e(u+v-uv)]\beta & 0 \\ 0 & [1-e(u+v-uv)]\beta - (\mu+\gamma) & 0 \\ 0 & \gamma & -\mu \end{pmatrix}.$$

Theorem 4.1. *(Matignon's Conditions) : An equilibrium point is locally asymptotically stable if* $|arg(\lambda_i)| > \alpha\frac{\pi}{2}$ *for all* λ_i*'s that are the eigenvalues of Jacobian matrix that evaluated at the equilibrium point [29].*

Theorem 4.2. *If* $\frac{[1-e(u+v-uv)]\beta}{\mu+\gamma} < 1$ *then* E_1 *is locally asymptotically stable.*

Proof. If all eigenvalues of $J(E_1)$ satisfy the Matignon's conditions then E_1 is locally asymptotically stable. Characteristic equation of $J|_{E_1}$ is found by using the relation $det(J|_{E_1} - \lambda I)$ where I is the identity matrix :

$$\begin{aligned} P(\lambda) &= \lambda^3 + (3\mu - [1-e(u+v-uv)]\beta + \gamma)\,\lambda^2 + (\mu^2 - 2\mu[1-e(u+v-uv)]\beta + 2\mu^2 + 2\mu\gamma)\lambda \\ &\quad + (-\mu^2[1-e(u+v-uv)]\beta + \mu^3 + \mu^2\gamma) = 0. \end{aligned}$$

Eigenvalues of $J|_{E_1}$ are found as:

- $\lambda_1 = -\mu$
- $\lambda_2 = -\mu$
- $\lambda_3 = -\mu + [1-e(u+v-uv)]\beta - \gamma$

According to Matignon's conditions, an equilibrium point is locally asymptotically stable if $|arg(\lambda_i)| > \alpha\frac{\pi}{2}$ for $i = 1, 2, 3$ where λ_i's are the eigenvalues of Jacobian matrix that evaluated at the equilibrium point. . Since all eigenvalues of $J|_{E_1}$ are real, all eigenvalues must be negative for the locally asymptotically stability. It is clear that λ_1 and λ_2 are already negative. If $\frac{[1-e(u+v-uv)]\beta}{\mu+\gamma} < 1$ satisfies, then λ_3 is negative.

□

Here, basic reproduction number for this model is obtained as $R_0 = \frac{[1-e(u+v-uv)]\beta}{\mu+\gamma}$.

Stability Conditions For E_2 **:** The Jacobian matrix is evaluated at E_2 in the following form :

$$\mathbf{J}|_{\mathbf{E_2}} = \begin{pmatrix} -\frac{\mu[1-e(u+v-uv)]\beta}{\mu+\gamma} & -(\mu+\gamma) & 0 \\ \frac{\mu[1-e(u+v-uv)]\beta}{\mu+\gamma} - \mu & 0 & 0 \\ 0 & \gamma & -\mu \end{pmatrix}.$$

Theorem 4.3. *(Fractional Routh Hurwitz Conditions): [30]*

- *Locally asymptotically stability conditions for the equilibrium point are* $a_1 > 0$, $a_3 > 0$, $a_1a_2 > a_3$ *if* $D\big(P(\lambda)\big) > 0$.
- *The equilibrium point is locally asymptotically stable for* $\alpha < \frac{2}{3}$ *if* $D\big(P(\lambda)\big) < 0$, $a_1 \geq 0$, $a_2 \geq 0$, $a_3 > 0$.
- *All roots of the characteristic equation of the endemic equilibrium point satisfy the condition* $|arg(\lambda_i)| < \alpha\frac{\pi}{2}$ *if* $D\big(P(\lambda)\big) < 0$, $a_1 < 0$, $a_2 < 0$ *and* $\alpha > \frac{2}{3}$.

Here, discriminant of the characteristic equation is as follows:

$$D\big(P(\lambda)\big) = 18a_1a_2a_3 + (a_1a_2)^2 - 4a_3a_1^3 - 4a_2^3 - 27a_3^2$$

where $P(\lambda)$ *in the following form:*

$$P(\lambda) = \lambda^3 + a_1\lambda^2 + a_2\lambda + a_3 = 0$$

Theorem 4.4. *Characteristic equation of $J|_{E_2}$ is found as follows :*

$$P(\lambda) = \lambda^3 + \left(\frac{\mu[1-e(u+v-uv)]\beta+\mu^2+\mu\gamma}{\mu+\gamma}\right)\lambda^2 + \left(\frac{2\mu^2[1-e(u+v-uv)]\beta+\mu[1-e(u+v-uv)]\beta\gamma-\mu^3-2\mu^2\gamma-\mu\gamma^2}{\mu+\gamma}\right)\lambda + \left(\frac{-\mu^4-2\mu^3\gamma+\mu^3[1-e(u+v-uv)]\beta+\mu^2[1-e(u+v-uv)]\beta\gamma-\mu^2\gamma^2}{\mu+\gamma}\right) = 0.$$

Discriminant of $P(\lambda)$ is found as follows :

$$D\big(P(\lambda)\big) = \frac{\mu^3\gamma^2\left(\mu-[1-e(u+v-uv)]\beta+\gamma\right)^2}{(\mu+\gamma)^4} + \frac{4\mu^3-4\mu^2[1-e(u+v-uv)]\beta+12\mu^2\gamma+\mu([1-e(u+v-uv)]\beta)^2}{(\mu+\gamma)^4} + \frac{-8\mu[1-e(u+v-uv)]\beta\gamma+12\mu\gamma^2-4[1-e(u+v-uv)]\beta\gamma^2+4\gamma^3}{(\mu+\gamma)^4}$$

Locally asymptotically stability conditions for E_2 are obtained as follows from the Fractional Routh Hurwitz Conditions:

- *Locally asymptotically stability conditions for the equilibrium point are* $\left(\frac{\mu[1-e(u+v-uv)]\beta+\mu^2+\mu\gamma}{\mu+\gamma}\right) > 0$, $\left(\frac{-\mu^4-2\mu^3\gamma+\mu^3[1-e(u+v-uv)]\beta+\mu^2[1-e(u+v-uv)]\beta\gamma-\mu^2\gamma^2}{\mu+\gamma}\right) > 0$, $\left(\frac{\mu[1-e(u+v-uv)]\beta+\mu^2+\mu\gamma}{\mu+\gamma}\right)\left(\frac{2\mu^2[1-e(u+v-uv)]\beta+\mu[1-e(u+v-uv)]\beta\gamma-\mu^3-2\mu^2\gamma-\mu\gamma^2}{\mu+\gamma}\right) > \left(\frac{-\mu^4-2\mu^3\gamma+\mu^3[1-e(u+v-uv)]\beta+\mu^2[1-e(u+v-uv)]\beta\gamma-\mu^2\gamma^2}{\mu+\gamma}\right)$ *if* $D\big(P(\lambda)\big) > 0$.

- *The equilibrium point is locally asymptotically stable for* $\alpha < \frac{2}{3}$ *if* $D\big(P(\lambda)\big) < 0$, $\left(\frac{\mu[1-e(u+v-uv)]\beta+\mu^2+\mu\gamma}{\mu+\gamma}\right) \geq 0$, $\left(\frac{2\mu^2[1-e(u+v-uv)]\beta+\mu[1-e(u+v-uv)]\beta\gamma-\mu^3-2\mu^2\gamma-\mu\gamma^2}{\mu+\gamma}\right) \geq 0$, $\left(\frac{-\mu^4-2\mu^3\gamma+\mu^3[1-e(u+v-uv)]\beta+\mu^2[1-e(u+v-uv)]\beta\gamma-\mu^2\gamma^2}{\mu+\gamma}\right) > 0$.

- *All roots of the characteristic equation of the endemic equilibrium point satisfy the condition* $|arg(\lambda_i)| < \alpha\frac{\pi}{2}$ *if* $D\big(P(\lambda)\big) < 0$, $\left(\frac{\mu[1-e(u+v-uv)]\beta+\mu^2+\mu\gamma}{\mu+\gamma}\right) < 0$, $\left(\frac{2\mu^2[1-e(u+v-uv)]\beta+\mu[1-e(u+v-uv)]\beta\gamma-\mu^3-2\mu^2\gamma-\mu\gamma^2}{\mu+\gamma}\right) < 0$ *and* $\alpha > \frac{2}{3}$.

5. Case studies for different parameter values

In this section, the basic reproduction numbers corresponding to various parameter values employed in the numerical results are calculated, and their stability is analyzed for both the disease-free equilibrium point and the endemic equilibrium point.

	μ	β	e	u	v	γ
Case i)	0.00972	0.09598	0.4	0.6769	0.6769	0.10890
Case ii) a)	0.00972	0.09598	0.1	0.8	0.8	0.10890
Case ii) b)	0.00972	0.09598	0.3	0.8	0.8	0.10890
Case ii) c)	0.00972	0.09598	0.5	0.8	0.8	0.10890
Case ii) d)	0.00972	0.09598	0.7	0.8	0.8	0.10890
Case ii) e)	0.00972	0.09598	0.9	0.8	0.8	0.10890
Case iii) a)	0.00972	0.09598	0.8	0.1	0.1	0.10890
Case iii) b)	0.00972	0.09598	0.8	0.3	0.3	0.10890
Case iii) c)	0.00972	0.09598	0.8	0.5	0.5	0.10890

Case iii) d)	0.00972	0.09598	0.8	0.7	0.7	0.10890
Case iii) e)	0.00972	0.09598	0.8	0.9	0.9	0.10890
Case iv) a)	0.00972	0.09598	0.8	0.1	0.2	0.10890
Case iv) b)	0.00972	0.09598	0.8	0.3	0.2	0.10890
Case iv) c)	0.00972	0.09598	0.8	0.5	0.2	0.10890
Case iv) d)	0.00972	0.09598	0.8	0.7	0.2	0.10890
Case iv) e)	0.00972	0.09598	0.8	0.9	0.2	0.10890
Case v) a)	0.00972	0.09598	0.8	0.2	0.1	0.10890
Case v) b)	0.00972	0.09598	0.8	0.2	0.3	0.10890
Case v) c)	0.00972	0.09598	0.8	0.2	0.5	0.10890
Case v) d)	0.00972	0.09598	0.8	0.2	0.7	0.10890
Case v) e)	0.00972	0.09598	0.8	0.2	0.9	0.10890

Table 2. Parameter values taken for each case

Since R_0 <1,locally asymptotically stability of disease free equilibrium point holds for all cases. For all cases $D\big(P(\lambda)\big) > 0$ and $a_3 < 0$,so endemic equilibrium point is unstable for these parameter values according to Fractional Routh Hurwitz Conditions.

	$D(P(\lambda))$	a_1	a_3	a_1a_2
Case i	0.00000000058068	0.0148	-0.0000053875	-0.0000074607
Case ii) a)	0.00000000010415	0.0168	-0.0000030095	-0.0000040478
Case ii) b)	0.00000000039990	0.0153	-0.0000047506	-0.0000066536
Case ii) c)	0.0000000010106	0.0138	-0.0000064916	-0.0000086741
Case ii) d)	0.0000000020525	0.0123	-0.0000082327	-0.000010109
Case ii) e)	0.0000000036433	0.0108	-0.0000099738	-0.000010959
Case iii) a)	0.00000000016466	0.0164	-0.0000035173	-0.0000048683
Case iii) b)	0.00000000073733	0.0144	-0.0000058388	-0.0000079850
Case iii) c)	0.0000000016038	0.0129	-0.0000075798	-0.0000096396
Case iii) d)	0.0000000024545	0.0119	-0.0000087405	-0.000010418
Case iii) e)	0.0000000029749	0.0114	-0.0000093209	-0.000010709
Case iv) a)	0.00000000027202	0.0158	-0.0000041702	-0.0000058500
Case iv) b)	0.00000000056276	0.0148	-0.0000053309	-0.0000073921
Case iv) c)	0.0000000010106	0.0138	-0.0000064916	-0.0000086741
Case iv) d)	0.0000000016500	0.0128	-0.0000076524	-0.0000096959
Case iv) e)	0.0000000025159	0.0118	-0.0000088131	-0.000010458
Case v) a)	0.00000000027202	0.0158	-0.0000041702	-0.0000058500
Case v) b)	0.00000000056276	0.0148	-0.0000053309	-0.0000073921
Case v) c)	0.0000000010106	0.0138	-0.0000064916	-0.0000086741
Case v) d)	0.0000000016500	0.0128	-0.0000076524	-0.0000096959
Case v) e)	0.0000000025159	0.0118	-0.0000088131	-0.000010458

Table 3. Obtained Values For Each Case

6. Numerical approximation method

Fractional Forward Euler Method is used for the model in this article .

Fractional Forward Euler Method : [31] Let the initial value problem be as follows:

$$\begin{cases} D^{\alpha} f(t) = \Big(g\big(t, f(t)\big)\Big) \\ f(0) = f_0 \end{cases} \tag{6.1}$$

and α is in the open interval (0,1) , t is in the closed interval $[0, t_g]$.

Caputo derivative is defined as

$$^{C}D_t^{\alpha} f(t) = \frac{1}{\Gamma(1-\alpha)} \int_0^t (t-s)^{-\alpha} f'(s) ds, \quad \alpha \in (0,1).$$

The solution of (6.1) which is found by using fractional forward Euler formula is as follows :

$$f_{k+1} = f_0 + h^{\alpha} \sum_{j=0}^{k} a_{j,k+1} g(t_j, f_j), \quad k = 0, 1, ..., K-1.$$

Here,

$$a_{j,k+1} = \frac{(k-j+1)^{\alpha} - (k-j)^{\alpha}}{\Gamma(1+\alpha)}, \quad k = 0, 1, ..., K-1, \quad j = 0, 1, ..., k.$$

The fractional forward Euler formula for the system (2.1) is obtained as

$$S_{k+1} = S_0 + h^{\alpha} \sum_{j=0}^{k} a_{j,k+1} \Big(\mu N - \mu S_j - \frac{[1 - e(u + v - uv)]\beta}{N} S_j I_j \Big)$$

$$I_{k+1} = I_0 + h^{\alpha} \sum_{j=0}^{n} a_{j,k+1} \Big(\frac{[1 - e(u + v - uv)]\beta}{N} S_j I_j - (\mu + \gamma) I_j \Big)$$

$$R_{k+1} = R_0 + h^{\alpha} \sum_{j=0}^{k} a_{j,k+1} \Big(\gamma I_j - \mu R_j \Big)$$

Here,

$$a_{j,k+1} = \frac{(k-j+1)^{\alpha} - (k-j)^{\alpha}}{\Gamma(1+\alpha)}, \quad k = 0, 1, ..., K-1, \quad j = 0, 1, ..., k.$$

7. Sensitivity analysis

Sensitivity indices quantify the relative change in a state variable resulting from a change in a given parameter. The normalized forward sensitivity index of a variable with respect to a parameter is defined as the ratio of the relative change in the state variable to the relative change in the parameter.

[39] The normalized forward sensitivity index of a variable that exhibits a differentiable dependence on a parameter is defined as follows:

$$\Upsilon_p^v := \frac{\partial v}{\partial p} . \frac{p}{v}$$

where v is a variable and p is a parameter.

Using this definition, the sensitivity indices of R_0 are determined separately for each of the six parameters as follows:

$$\Upsilon_{\mu}^{R_0} = -\frac{\mu}{\mu + \gamma},$$

$$\Upsilon_{\beta}^{R_0} = +1,$$

$$\Upsilon_{e}^{R_0} = -\frac{e(u + v - uv)}{1 - e(u + v - uv)},$$

$$\Upsilon_{u}^{R_0} = -\frac{(1 - v)eu}{1 - e(u + v - uv)},$$

$$\Upsilon_{v}^{R_0} = -\frac{(1 - u)ev}{1 - e(u + v - uv)},$$

$$\Upsilon_{\gamma}^{R_0} = -\frac{\gamma}{\mu + \gamma}.$$

8. Graphically enhanced numerical results: Data fitting and comparative study

The initial conditions are taken as S_0=80235597 , $I_0 = 601990$, $R_0 = 3842686$ to plot the figures in this section by considering real data for Türkiye from 21 April 2021 to 30 April 2021 [32]. The birth and death rate is taken as the average of birth and death rate in Türkiye in 2021 [33],[34]. So μ is taken as μ= 0.00972 and N=84680273 [35] in the calculations.

8.1 Data fitting

The best data fitting of the model that used in this article is done by using real data for Türkiye from 21 April 2021 to 30 April 2021.

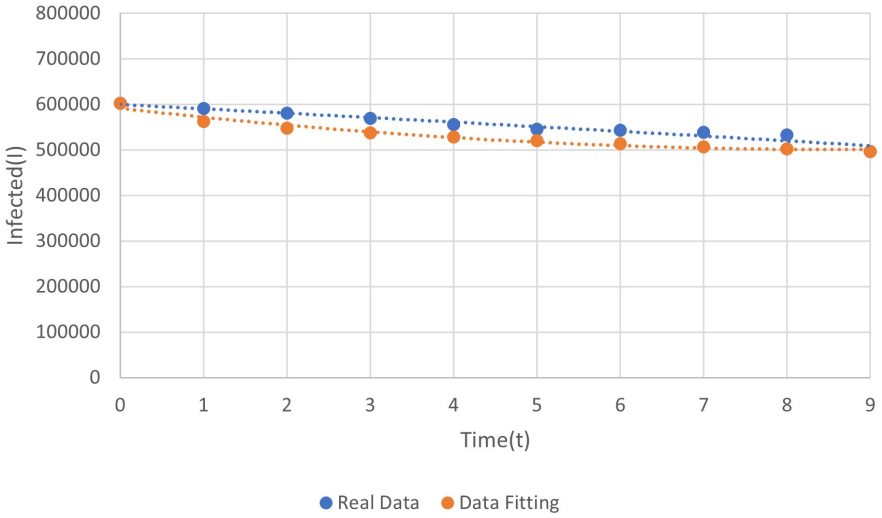

Figure 2. Data Fitting

In the next figure, the obtained data and the real data are given and the results are compared:

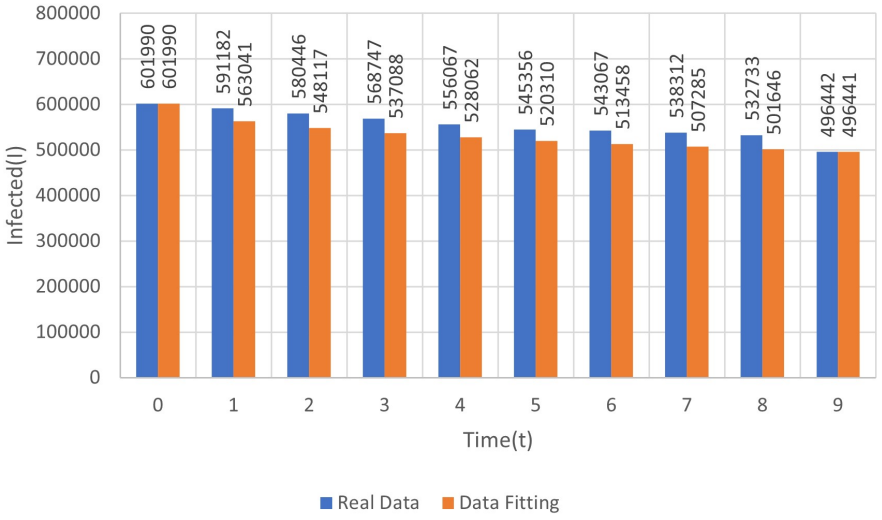

Figure 3. Comparison For Data Fitting Of Model

The best data fitting of the model is done for the following estimated parameters :

Parameter	Estimated Value
β	0.09598
γ	0.10890
e	0.4
u	0.6769
v	0.6769

Table 4. Estimated Parameter Values that Used for Best Data Fitting

The values of the sensitivity indices for each of the parameters considered in the data fitting process are provided separately as follows:

$$\Upsilon_{\mu}^{R_0} = -0.08194233687, \qquad \Upsilon_{\beta}^{R_0} = +1,$$

$$\Upsilon_{e}^{R_0} = -0.5582211151, \qquad \Upsilon_{u}^{R_0} = -0.136317166,$$

$$\Upsilon_{v}^{R_0} = -0.136317166, \qquad \Upsilon_{\gamma}^{R_0} = -0.9180576631.$$

8.2 Comparisons by taking different e, u, v values

Comparison 1: In Figure 5 plots with $\beta = 0.09598$, $\gamma = 0.10890$, $\alpha = 0.8$ and $u = v = 0.8$ are given.

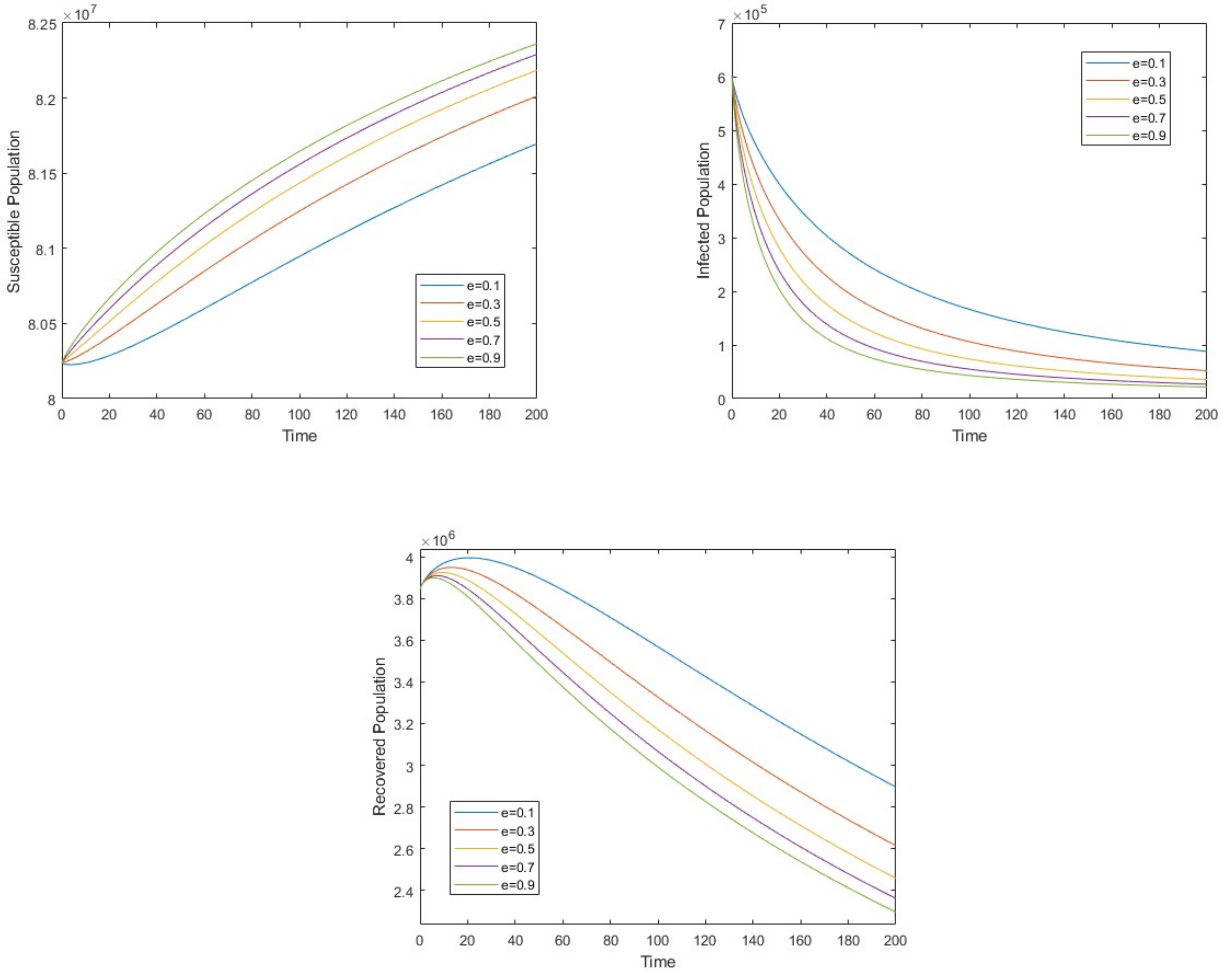

Figure 5. Comparison 1

Comparison 2: In Figure 7 plots with $\beta = 0.09598$, $\gamma = 0.10890$, $\alpha = 0.8$ and $e = 0.8$ are given.

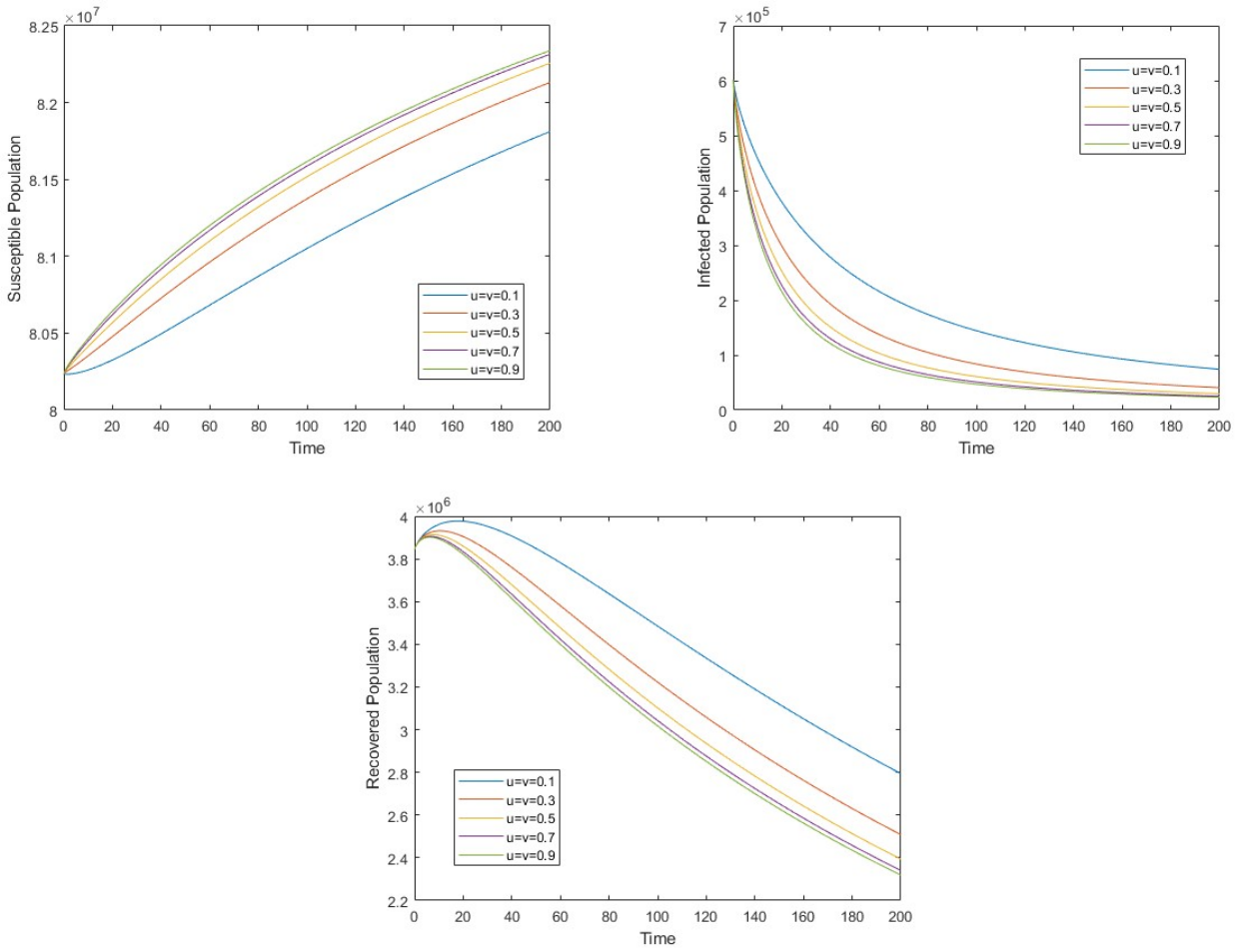

Figure 7. Comparison 2

Comparison 3: In Figure 9 plots with $\beta = 0.09598$, $\gamma = 0.10890$, $\alpha = 0.8$, $e = 0.8$, $v = 0.2$ are given.

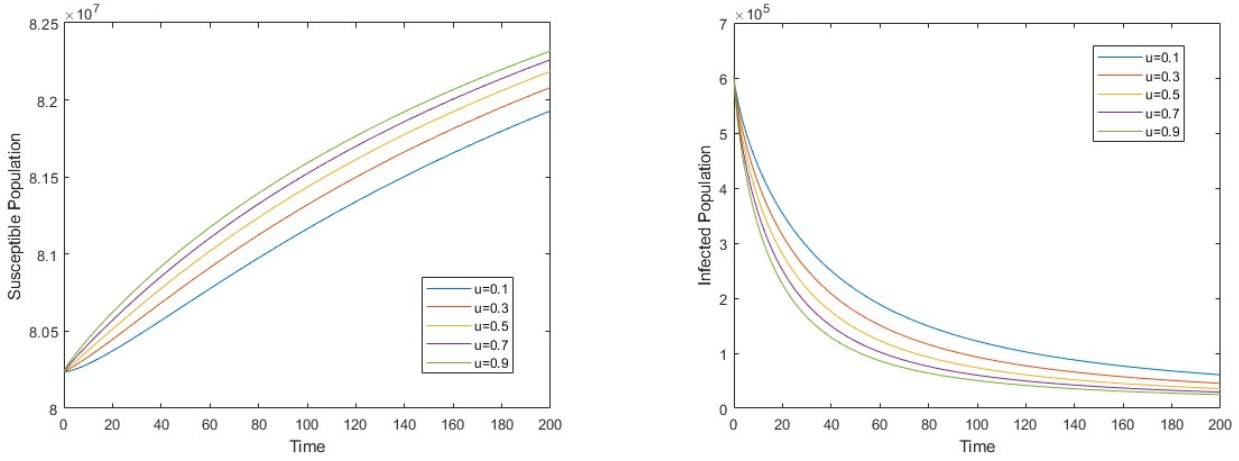

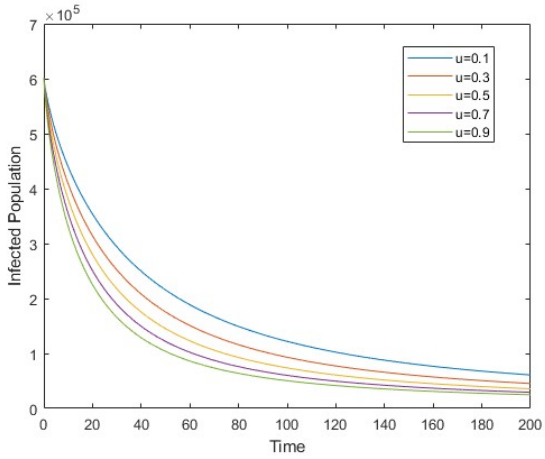

Figure 9. Comparison 3

Comparison 4: In Figure 11 plots with $\beta = 0.09598$, $\gamma = 0.10890$, $\alpha = 0.8$, $e = 0.8$ and $u = 0.2$ are given.

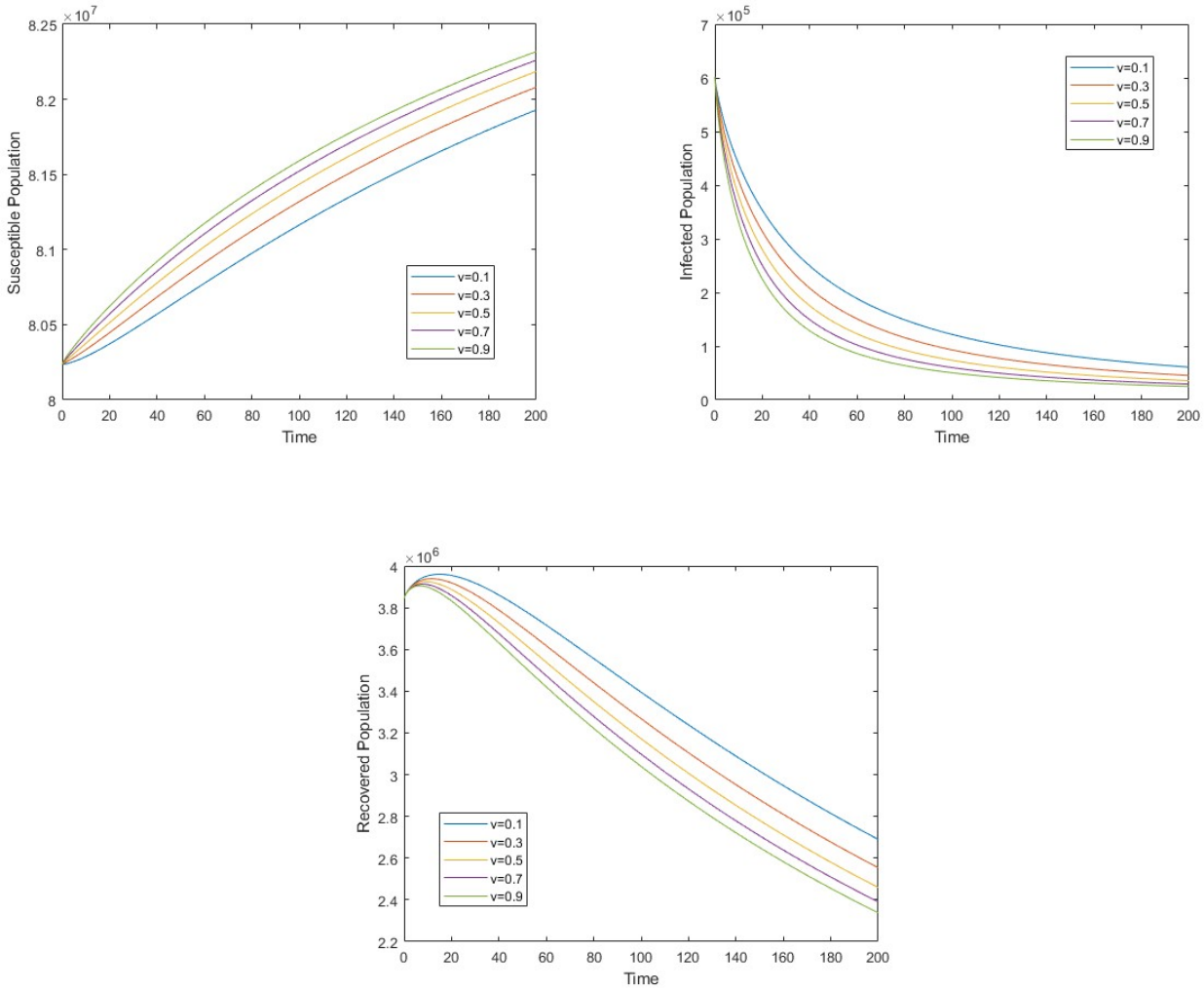

Figure 11. Comparison 4

9. Conclusion

In this study, we developed a fractional SIR model characterized by meticulously selected parameters. The mathematical properties of the model, including stability analysis, were rigorously examined. Subsequently, to align the model's objectives with empirical data, we conducted data fitting and comparative analyses utilizing actual Covid-19 statistics from Türkiye for the periods of April 21, 2021, and April 30, 2021. The data fitting process addressed the critical question: "What was the mask-wearing rate during the specified periods in Türkiye?".

Furthermore, the impact of varying rates of mask-wearing and mask efficiency on the number of infected individuals was analyzed through a series of comparative assessments.

Comparison 1 examined the effect of varying mask efficiency (e) while holding all other parameters constant. The results indicated that an increase in mask efficiency significantly reduces the number of infected individuals, underscoring the critical importance of wearing effective masks.

Comparison 2 involved adjusting the rates of mask-wearing (u) and the efficiency of mask-wearing (v) while maintaining other parameters constant, specifically by setting $u = v$. The findings revealed that an increase in the rates of mask-wearing correlates with a reduction in the number of infected individuals.

Comparison 3 analyzed the impact of varying the rate of mask-wearing (u) while keeping all other parameters constant. In Comparison 4, the focus shifted to adjusting the rate of mask efficiency (v), again with all other parameters held constant. Notably, the results from Comparisons 3 and 4 demonstrated identical values for the susceptible (S), infected (I), and recovered (R) populations when considered concurrently. This observation highlights that the significance of mask-wearing is equally pertinent for both susceptible and infected individuals.

Article Information

Acknowledgements: The authors are grateful to The Scientific and Technological Research Council of Türkiye (TUBITAK) for their financial support within the scope of "2211-E (2024/2) Direct Domestic PhD Scholarship Programme" .

Author's contributions: Elif Demir contributed to the conceptualization of the study, methodology design, validation of the results, formal analysis, provision of resources, review and editing of the manuscript, academic supervision, and project administration. Canan Vural contributed to the conceptualization of the study, methodology design, software development, literature investigation, formal analysis, preparation of the original draft of the manuscript, and visualization.

Artificial Intelligence Statement: The authors declare that no generative artificial intelligence (AI) tools or AI-assisted technologies were used in the writing, editing, data analysis, or any other part of this manuscript. All results, analyses, and textual content were produced solely by the authors.

Conflict of Interest Disclosure: No potential conflict of interest was declared by authors.

Plagiarism Statement: This article was scanned by the plagiarism program.

References

[1] Republic of Türkiye Ministry of Health: First Covid-19 Case in Turkey, https://covid19.saglik.gov.tr/Eklenti/39551/0/ covid-19rehberigenelbilgilerepidemiyolojivetanipdf.pdf

[2] Republic of Türkiye Ministry of Health: General Information About Covid-19, https://covid19.saglik.gov.tr/TR-66300/covid-19-nedir-.html

[3] Republic of Türkiye Ministry of Health: Social Distance, https://covid19.saglik.gov.tr/TR-66516/sosyal-mesafe.html

[4] Republic of Türkiye Ministry of Health: Protection From Covid-19, https://www.seyahatsagligi.gov.tr/site/KoronaVirusKorunma

[5] Ju, J. T., Boisvert, L. N., Zuo, Y. Y.: *Face masks against Covid-19: Standards, efficacy, testing and decontamination methods.* Advances in Colloid and Interface Science. **292**, 102435 (2021).

[6] Baleanu, D., Diethelm, K., Scalas, E., Trujillo, J. J.: Fractional Calculus: Models and Numerical Methods. World Scientific, (2012).

[7] Sadki, M., Harroudi, S., Allali, K.: *Fractional-order SIR epidemic model with treatment cure rate.* Partial Differential Equations in Applied Mathematics. **8**, 100593 (2023).

[8] Hamdan, N. I., Kilicman, A.: *A fractional order SIR epidemic model for dengue transmission.* Chaos, Solitons & Fractals. **114**, 55–62 (2018).

[9] Baba, I. A., Nasidi, B. A.: *Fractional order model for the role of mild cases in the transmission of Covid-19.* Chaos, Solitons & Fractals. **142**, 110374 (2021).

[10] Alshomrani, A. S., Ullah, M. Z., Baleanu, D.: *Caputo SIR model for Covid-19 under optimized fractional order.* Advances in Difference Equations. **2021** (1), 185 (2021).

[11] Nenoff, L., Ribeiro, C. O., Matter, M., Hafner, L., Josipovic, M., Langendijk, J. A., Persson, G. F., Walser, M., Weber, D. C., Lomax, A. J., Knopf, A. C., Albertini, F., Zhang, Y.: *Deformable image registration uncertainty for inter-fractional dose accumulation of lung cancer proton therapy.* Radiotherapy and Oncology. **147**, 178–185 (2020).

[12] Magin, R. L.: *Fractional calculus models of complex dynamics in biological tissues.* Computers & Mathematics with Applications. **59** (5), 1586–1593 (2010).

[13] Mishra, J.: *Telegraph model with fractional differential operators: Nonsingular kernels.* Results in Physics. **39**, 105762 (2022).

[14] Sun, H., Chen, W., Li, C., Chen, Y.: *Fractional differential models for anomalous diffusion.* Physica A: Statistical Mechanics and its Applications. **389** (14), 2719–2724 (2010).

[15] Rehman, H., Shuaib, M., Ismail, E. A., Li, S.: *Enhancing medical ultrasound imaging through fractional mathematical modeling of ultrasound bubble dynamics.* Ultrasonics Sonochemistry. **100**, 106603 (2023).

[16] Raza, A., Khan, S. U., Al-Khaled, K., Khan, M. I., Haq, A. U., Alotaibi, F., Abd Allah, A. M., Qayyum, S.: *A fractional model for the kerosene oil and water-based Sasson nanofluid with inclined magnetic force.* Chemical Physics Letters. **787**, 139277 (2022).

[17] Liang, S., Luo, R., Luo, W.: *Fractional differential constitutive model for linear viscoelasticity of asphalt and asphalt mastic.* Construction and Building Materials. **306**, 124886 (2021).

[18] Di Paola, M., Pinnola, F. P., Zingales, M.: *Fractional differential equations and related exact mechanical models.* Computers & Mathematics with Applications. **66** (5), 608–620 (2013).

[19] Karaman, B., Karaman, E.: *The mathematical dynamics of the Caputo fractional order social media addiction design.* Communications in Advanced Mathematical Sciences. **8** (1), 1-10 (2025).

[20] Demir, İ., Kirisci, M.: *Forecasting COVID-19 Disease Cases Using the SARIMA-NNAR Hybrid Model.* Universal Journal of Mathematics and Applications. **5** (1), 15-23 (2022).

[21] Tsega, E.: *Fitting an epidemiological model to transmission dynamics of COVID-19.* Journal of Mathematical Sciences and Modelling. **3** (3), 135-138 (2020).

[22] Ahmad, Z., Khan, N., Arif, M., Murtaza, S., Khan, I.: *Dynamics of fractional order SIR model with a case study of covid-19 in Turkey.* City University International Journal of Computational Analysis. **4** (1), 18–35 (2020).

[23] Aziz, M. M., Mahmood, A. S.: *Analysis of dynamical behavior for epidemic disease covid-19 with application.* Turkish Journal of Computer and Mathematics Education (TURCOMAT). **12** (4), 568–577 (2021).

[24] Bagal, D. K., Rath, A., Barua, A., Patnaik, D.: *Estimating the parameters of susceptible-infected-recovered model of Covid-19 cases in India during lockdown periods.* Chaos, Solitons & Fractals. **140**, 110154 (2020).

[25] Farman, M., Akgül, A., Ahmad, A., Baleanu, D., Umer Saleem, M.: *Dynamical transmission of coronavirus model with analysis and simulation.* Computer Modeling in Engineering & Sciences. **127** (2), 753–769 (2021).

[26] Kumar, R., Kumar, S.: *A new fractional modelling on susceptible-infected-recovered equations with constant vaccination rate.* Nonlinear Engineering. **3** (1), 11–19 (2014).

[27] Alshammari, F. S., Khan, M. A.: *Dynamic behaviors of a modified SIR model with nonlinear incidence and recovery rates.* Alexandria Engineering Journal. **60** (3), 2997–3005 (2021).

[28] Odibat, Z. M., Shawagfeh, N. T.: *Generalized Taylor's formula.* Applied Mathematics and Computation. **186** (1), 286–293 (2007).

[29] Matignon, D.: *Stability results for fractional differential equations with applications to control processing.* In: Computational Engineering in Systems Applications, Lille, France. **2**, 963–968 (1996).

[30] Ahmed, E., El-Sayed, A., El-Saka, H. A.: *On some Routh–Hurwitz conditions for fractional order differential equations and their applications in Lorenz, Rössler, Chua and Chen systems.* Physics Letters A. **358** (1), 1–4 (2006).

[31] Tomášek, P.: *On Euler methods for Caputo fractional differential equations.* Archivum Mathematicum. **59** (3), 287–294 (2023).

[32] Republic of Türkiye Ministry of Health: General Covid-19 Table in Turkey, https://covid19.saglik.gov.tr/TR-66935/genel-koronavirus-tablosu.html

[33] Turkish Statistical Institute: Birth Rate in Turkey For 2021, https://data.tuik.gov.tr/Bulten/Index?p=Birth-Statistics-2021-45547

[34] Turkish Statistical Institute: Death Rate in Turkey For 2021, https://data.tuik.gov.tr/Bulten/Index?p=lm-ve-lm-Nedeni-statistikleri-2021-45715&dil=1

[35] Turkish Statistical Institute: Population of Turkey in 2021, https://data.tuik.gov.tr/Bulten/Index?p=Population-and-Housing-Census-2021-45866

[36] Vural, C.: On SIR Models with Fractional Derivatives, Master Thesis. Yildiz Technical University, (2024).

[37] Alqahtani, R. T.: *Mathematical model of SIR epidemic system (Covid-19) with fractional derivative: Stability and numerical analysis.* Advances in Difference Equations. **2021** (1), 2 (2021).

[38] Mahata, A., Paul, S., Mukherjee, S., Das, M., Roy, B.: *Dynamics of Saputo fractional order SEIRV epidemic model with optimal control and stability analysis.* International Journal of Applied and Computational Mathematics. **8** (1), 28 (2022).

[39] Chitnis, N., Hyman, J. M., Cushing, J. M.: *Determining important parameters in the spread of malaria through the sensitivity analysis of a mathematical model.* Bulletin of Mathematical Biology. **70**, 1272–1296 (2008).

Affiliations

ELIF DEMIR
ADDRESS: Yildiz Technical University, Department of Mathematics, 34220, Istanbul-Türkiye
E-MAIL: edbilek@yildiz.edu.tr
ORCID ID: 0000-0001-5973-9115

CANAN VURAL
ADDRESS: Istanbul University, Department of Mathematics, 34134, Istanbul-Türkiye
E-MAIL: canan.vural@istanbul.edu.tr
ORCID ID: 0009-0000-6631-0085